Numerical Simulation of Heat Affected Zone Microstructure During Laser Surface Melting

M.Amin Jabbareh[a], H. Asadi[*b]
[a](Ph.D. student), Tarbiat Modares University, Department of Materials Engineering, Tehran, Iran
[b] (Prof.), Tarbiat Modares University, Department of Materials Engineering, Tehran, Iran

ARTICLE INFO

Article history:

Received 24 Aug 2012
Accepted 5 Jan 2013
Available online 20 November 2013

Keywords:

Laser surface melting
Microstructure
Heat affected zone
Phase field simulation.

ABSTRACT

Microstructural changes during laser welding and laser surface treatment has been regarded by many researchers. Most researches have focused on studying the effect of various process parameters on the size and microstructure of the heat affected zone. But some studies show that the initial microstructure of the base metal can also affect the heat affected zone dimensions and final microstructure. In this research, the effect of initial grain size on final microstructure of the heat affected zone in laser surface melting process has been studied. For this purpose we used phase field simulation technique. The results showed that the change in initial grain size can lead to a change in the size of the heat affected zone and grain topology in this area.

1. Introduction

Nowadays, lasers have numerous applications in a variety of industries such as aerospace and automotive industries [1-3]. The main uses of lasers in industrial processes include welding process [4], machining and cutting processes [5,6] and surface treatments [7]. Although narrow heat affected zone (HAZ) is one of the main advantages of using lasers in such processes, but still HAZ formation in laser-related processes can lead to the decrease of mechanical properties of the material [8]. This is mainly due to grain growth and phase transformations in the HAZ [9, 10]. Hence, in order to control the microstructure and size of the HAZ, and also to identify the parameters controlling these two factors, extensive studies have been carried out. For instance, Zhao et al. [8] studied the effect of cooling rate and peak temperature on the microstructure, hardness and fracture toughness of heat affected zone during laser welding of high nitrogen steels. Valette et al. [11] and Singh et al. [12] investigated the effect of pulse duration and scanning speed on HAZ dimensions in laser cutting processes, respectively. Benyounis et al. [13] presented a mathematical model to study the effect of laser power and welding speed on the heat input and HAZ dimensions. Combining Monte Carlo and finite element method, Kong et al. [14] investigated the effect of laser scanning speed on the grain size and percentage of different phases in the HAZ of laser surface heat treated dual phase steel.
Furthermore, the effects of laser power, laser scan speed and laser diameter on HAZ dimensions in laser-assisted machining were investigated [15].According to the literature, heat input, peak temperature, cooling rate, scanning speed, heat source power, laser duration and beam diameter are the most important parameters that their impact on the microstructure and size of the HAZ has been studied.

Corresponding author:
E-mail address: ha10003@modares.ac.ir (Hamid Asadi).

As can be seen in all of these studies, only the process parameters are taken into consideration. However, by simulating the recrystallization and grain growth in the HAZ of gas tungsten arc welded steel,Thiessen et al. [16] showed that if the initial grain size distribution in the experimental and simulation samples are the same, the predicted grain size distribution in the HAZ is acceptable, while the different distribution of the grain size in the experimental and simulation samples causesgreat difference between numerical and experimental results. These results show that the initial microstructure of specimen can affect the final microstructure of the HAZ, which has been less considered.

In this study we aim to further explore the effect of initial grain size on microstructure and dimensions of HAZ during single pulse laser surface melting process of a pure material. For this purpose a phase field model capable of simulating polycrystalline structures was used.

2. Materials and research methodology

2.1. Phase field model

In this study, the phase field approach was used to simulate the microstructure evolution during laser surface melting process. The details of the method have been presented in [17]. Briefly, in this method, like as well as temperature and/or concentration the system phase is defined as a field variable, too. Phase field variable is defined in such a way that it continuously changes between two fixed values (e.g. 0 and 1). Thus, each of these fixed values is defined as solid and liquid phases and the transition between the values attributed to the solid / liquid interface. Then the energy function of the system (F) is defined based on the phase field variable and other field variables such as temperature and concentration. By minimizing this function according to equation (1), the stable phase at any point in the system at any time is characterized.

$$\partial\phi/\partial t = -M_{\phi}(\delta F/\delta t) \qquad (1)$$

Whereϕ is phase field variable, t is time, M_{ϕ} is the interface mobility and F is the energy function of the system. To simulate microstructural changes during thermal processes, the above equation is solved simultaneously with the equations of heat and/or mass transfer.

Modeling of microstructure evolution in this work is based on the standard phase-field approach for solidification modeling [17] with probabilistic algorithm for the evolution of crystal orientation. In this model the free energy functional of the system has the following form

$$F = \int \left[f(\phi, T) + \frac{1}{2}\varepsilon_{\phi}^{2}|\nabla\phi|^{2} + g \right] dV \qquad (2)$$

Where$f$ is the local volumetric free energy density, ε_{ϕ} is a constant relating to the solid/liquid interface thickness, and g is an energy term encapsulating the free energy of the crystallographic mismatch between the given control volume and its neighbors. Details of the model have been described in [18,19]. The evolution of orientation is worked out through a Monte-Carlo algorithm. According to this algorithm, the probability of change of orientation to a randomly selected new orientation is given as

$$pr = p_0 \exp\left(-\frac{Q}{RT}\right)\left(1 - exp\left[\frac{k(g_{new}-g_{old})}{RT}\right]\right) \qquad (3)$$

Where$k$ and p_0 are constant coefficient, Q is activation energy for grain boundary migration *and* g_{old} and g_{new} are the mismatch energies of the original and the new orientation of the given cell, respectively. Subsequently, a random number, r, is generated in the range 0-1. The new orientation is accepted if $r<pr$.

Note that the probability in Eq. (3) consists of two terms. The first term corresponds to the mobility of grain boundaries, which increases with increasing temperature, and the second term corresponds to the thermodynamic driving force for grain boundary migration, which is mainly governed by the orientational mismatch between the adjacent grains. With this definition, the variation of pr with temperature may take many different forms, depending on the value of constant coefficients (k and p_0) and Q.As shown in

Figure 1, in this study the parameters were set in such a way that *pr* tends to zero at temperatures lower than T/T_m=0.5 (i.e. lack of grain growth) and rapidly increases by increasing temperature. Finally in temperatures near the melting point, maximum values of *pr* are obtained. The parameters used to specify grain growth kinetics are presented in Table 1.

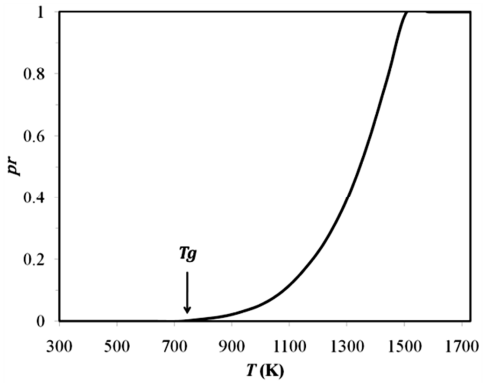

Fig.1. Variation of orientation selection probability with temperature

Table1. Input parameters for grain growth kinetic equation (Eq.3)

Parameter	Symbol	Value	Unit
Activation energy	Q	782	J/mol
Driving force multiplier	k	400	-
Kinetic multiplier	p_0	100	-

2.2. Numerical simulation

An explicit, isotropic finite difference scheme is used to work out the temporal evolutions of the phase and the temperature fields. Numerical simulations were performed in two dimension domains with 650 × 300 grid, with a grid spacing of 1500 nm, and a time increment of 20 ns. Thermal cycle of single pulse of laser processes applied to the system as a heat flux boundary condition on 400 cell of the top surface of simulation domain (which is indicated the laser diameter) with duration of 5×10^{-5} second and insulating boundary conditions were applied to other parts of domain boundary. Figure 2 shows a schematic diagram of simulation domain.

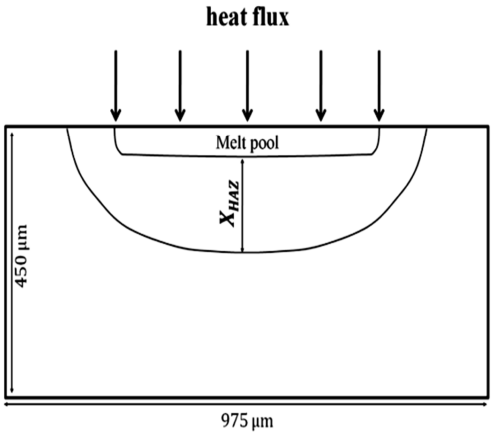

Fig.2. Schematic diagram of simulation domain

To study the effect of initial grain size on the final grain structure of HAZ, four initial microstructures with average grain size of 10, 20, 35 and 45 µm were created, using different nucleation and growth conditions. According to the probabilistic nature of grain growth [20], four samples of each microstructure, with different grains orientation and equal average grain size were created and used as phase field initial condition in the next step of simulation (i.e. simulation of laser surface treatment) and the average calculated results were reported. In this study, thermodynamic properties of pure nickel were used. The values of these parameters are presented in Table 2.

Table2. Thermodynamic parameters used in numerical simulations.

Parameter	Symbol	Value	Unit
Heat diffusivity	α	2.3×10^{-5}	m^2/s
Melting point	T_m	1728	K
Latent heat of fusion	H	2.67×10^{9}	J/m^2
Heat capacity	c	4.8	$MJ/K/m^3$
Interface mobility	M_φ	0.007	m/s/K
Solid/liquid interface thickness	ε_ϕ	500	nm

2.3. HAZ criteria

Initially it is necessary to provide a clear definition of the HAZ. In this study (due to purity of the system), the only possible change in the microstructure of HAZ is grain growth. Thus, the heat affected zone boundary was defined by the degree of grain growth. It is assumed that a region belongs to HAZ if there is 20% or more increase in the mean grain size. Accordingly, a threshold grain size is defined as follows

$$d_{HAZ} = 1.2d_0 \quad (4)$$

To calculate the average grain size, the linear intercept method based on ASTM E112 was used.

2.4. Experimental procedure

In this investigation, commercially pure nickel was used as substrate for laser melting processing. The nickel plates with the thickness of 4 mm and two different initial grain sizes were treated by Nd: YAG pulsed laser with 5×10^8 W/m^2 power density, 5 ms pulse duration and 0.6 mm beam diameter. Optical metallography was performed on samples using conventional polishing and etching techniques.

3. Results and discussion

Figure 3 shows the simulated final grain structure of the melted zone and heat affected zone in comparison with experimental samples, for two different initial grain sizes. Comparison of Figure 3a and 3b reveals that an increase in initial grain size leads to a decrease in the depth of HAZ. This is consistent with the simulated microstructures (Figure 3c and 3d). These results indicate that in addition to the process parameters, initial grain size can also affect the formation of heat affected zone. The results also indicate the ability of the model to simulate complex microstructure evolution including solidification and grain growth simultaneously.

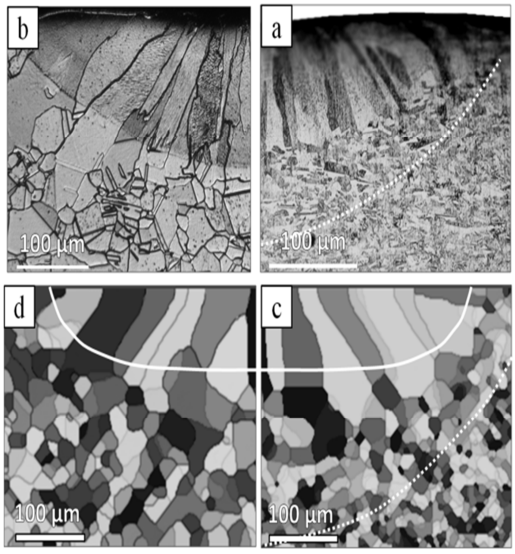

Fig.3. Experimental (a, b) and simulated (c, d) grain structure of melt pool and HAZ for specimens with fine (a, c) and coarse (b, d) initial grain sizes. Solid lines indicate the ultimate melt pool boundaries and dotted lines indicate boundaries of HAZ.

Figure 4 shows the simulated microstructure of melt pool and HAZ for different initial grain sizes and constant laser power density (P=35×10^9 W/m^2). Solid lines indicate melted region and dashed lines represent the thermal boundary of HAZ i.e. minimum temperature required to initiate grain growth (Tg in Fig.1).As can be seen, with increasing initial grain size, the microstructure of HAZ approached to the base metal microstructure, thus the difference between the base metal and the heat affected zone microstructure disappeared in Fig. 4d. While heat transfer conditions are the same in all cases, estimation of HAZ dimensions based on temperature isotherms leads to significant errors.

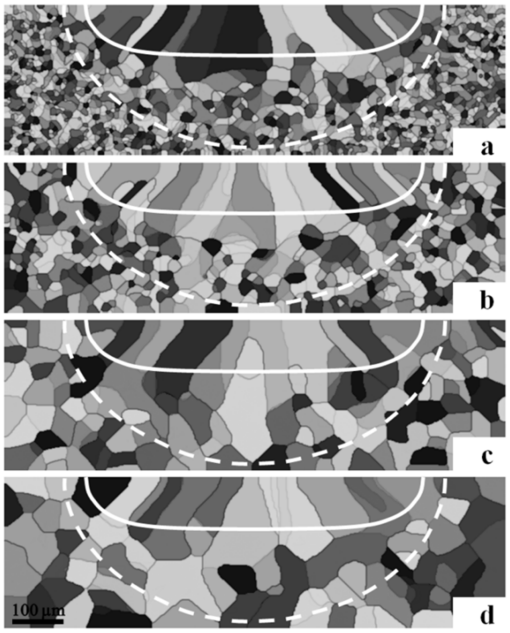

Fig.4. Simulated microstructure of melt pool and heat affected zone, a) d_0=10 µm, b) d_0=20 µm, c) d_0=35 µm, d) d_0=45 µm

Grain size distribution in various distances from the surface for systems with different initial grain sizes is shown in Figure 5. For better comparison, the grain size is normalized with respect to the initial grain size. Note that the horizontal lines are used to determine the grain size, so the calculated grain size in the weld pool shows the grain width in this area. As can be seen, the grains width is almost constant through the melt pool; but with distance from the surface and getting into the base metal the grain size gradually decreases and finally reaches the value d_0 for each sample. Similar results are reported in other studies [21]. The interesting point here is the dependence of grain growth degree on the initial grain size. In fine grained samples (d_0=10 µm), the grain size just below the melt pool (125 µm from the surface) is about three times greater than initial grain size, while by increasing initial grain size to 45 µm, this value is reduced to about 1.2. Another point is that in coarse grained samples the width of melt pool grains is approximately equal to the initial grain size of base metal. But with decreasing initial grain size, the difference between melt pool and base metal grain size greatly enhances. This is due to the fact that in fine grained structures, grain growth begins from the early stages of the process (i.e. melting stage). Thus, the freezing process actually starts from the grains which are much greater than initial ones. Whereas in coarse grained structures due to the lower energy level of the system, grain growth starts later and hence the grain size at the beginning of solidification process is not much different from the initial grain size. It should be noted that the nucleation of new grains in the melt pool has not been considered in these simulations. If we consider an alloy system with the possibility of grain nucleation in melt pool during solidification, final microstructure can be greatly different and decreasing of grain size, compared with the initial microstructure, is possible.

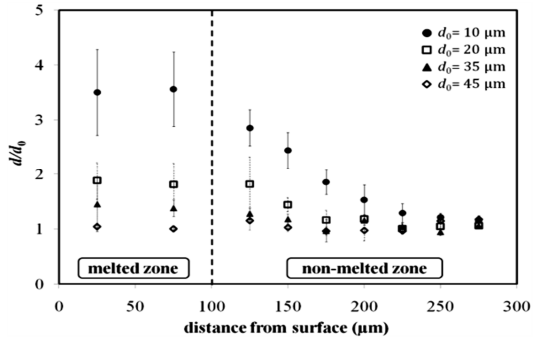

Fig.5. Distribution of normalized grain size in various distances from surface

Figure 6 shows the calculated depth of HAZ as a function of initial grain size for three different laser power densities. As can be seen, for a constant initial grain size, increasing power density increases the thickness of HAZ. This can be explained considering heat transfer situations. With increasing laser power density, more heat accumulates to the sample so the temperature rises up in a greater area of the specimen which leads to greater HAZ. In addition, it can be seen that in smaller initial grain size, increasing power density causes a further increase in the thickness of HAZ. This is probably because grain growth in fine grained structures is more sensitive to temperature [22], thus small difference in temperature

leads to great difference in final grain size and HAZ dimensions. The results also show that in all laser power densities variation of HAZ depth versus initial grain size follows a logarithmic function. So for a constant power density, HAZ thickness is reduced with increasing initial grain size and finally reaches to zero in a critical initial grain size. This can be explained with regards to the increase in required driving force for grain growth with increasing initial grain size. Therefore in specific thermal conditions the value of grain growth in coarse grained systems is less;therefore HAZ thickness is smaller.

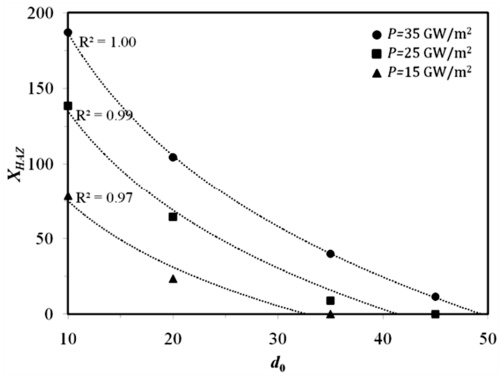

Fig.6. Calculated depth of HAZ as a function of initial grain size for various laser power densities

Calculated critical grain size for each laser power density is shown in Figure 7.The critical initial grain size is a linear function of the power density. Bellow this critical point, the assumed criterion HAZ detection, i.e. $d>1.2\ d_0$, is satisfied and a noticeably large area of coarse grains appears in the specimen. On the other hand, if the grain size is bigger than the critical value, the criterion is not satisfied anywhere and the extent of HAZ becomes negligible. From the slope of the curve it can be seen that a wider range of power densities can be used for coarse grained specimens without the risk of HAZ formation. For example, for a system with 40 µm initial grain size, maximum power density to prevent HAZ formation is 25 GW/m^2, while it becomes 38 GW/m^2 for a system with 50 µm initial grain size.

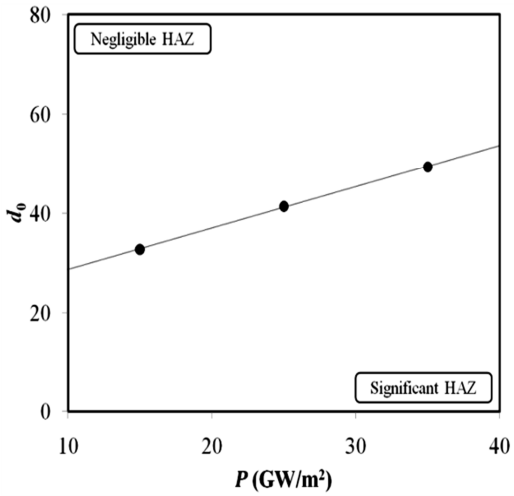

Fig.7. Variation of critical grain size versus laser power density

Figure 8 shows topological class distributions in HAZ in comparison with topological class distributions in base metal for two different initial grain sizes. In this diagram, the horizontal axis represents the number of neighbors for a specific grain and the vertical axis shows the proportion of grains having a specific number of neighbors. As can be seen, all four curves exhibit a quasi-normal distribution. For both samples, either in base metal or heat affected zone, the peak of frequency appears on neighboring number of five. Although the value of maximum frequency is different in each initial grain size, in both cases the formation of heat affected zone reduces the maximum value of frequency. For example, HAZ formation reduced the value of maximum frequency of base metal from 0.32 to 0.27 and 0.22 to 0.20 for 20 and 45 µm initial grain size, respectively. Increases of the width of HAZ curves to the smaller neighboring numbers in comparison with base metal curves show that the reduction of frequency value is probably due to the shrinkage of small grains and thus reduction of their neighboring number during grain growth. However, thetrend of topological changes from base metal to HAZ is the same in both initial grain sizes and indicates that the change in the initial grain size does not affect the topological changes.

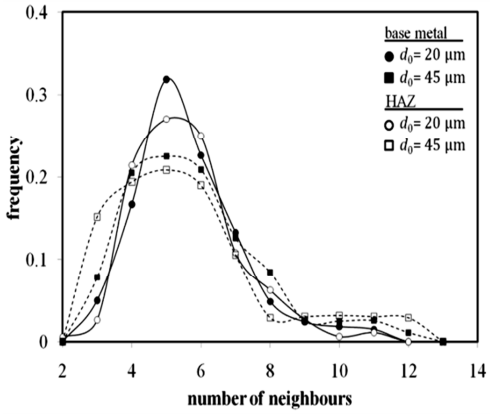

Fig.8. Topological class distributions in base metal and HAZ for two different initial grain sizes

4. Conclusions

Using phase field simulation technique, microstructural evolution of heat affected zone and weld pool during single pulse laser surface melting of a pure metal was simulated and the effect of initial grain size on formation of the HAZ was studied. The results indicated that the thickness of HAZ is a logarithmic function of initial grain size and increasing initial grain size decreases the thickness of HAZ. The results also showed that for each specific laser power density we can find a critical initial grain size in which the HAZ thickness reaches to zero. It was also identified that the broader range of laser power densities can be used for specimens with larger initial grain size, without the risk of HAZ formation. The results indicated that although the change in initial grain size leads to change the topological class distributions in base metal and HAZ but the trends of topological changes from base metal to HAZ is similar in all cases. Considering that the surface melting and solidification is the basis of all welding and surface treatment processes, these results could provide a basis for understanding and controlling the factors that influence microstructure and dimensions of the HAZ.

5. Acknowledgement

The authors are thankful to Dr. IrajHadi for his assistance with the experiments.

References

[1] Y. S. Yang, S. H. Lee, "A study on the joining strength of laser spot welding for automotive applications," Journal of Materials Processing Technology, vol. 94, 1999, pp. 151–156.

[2] J. D. Damborenea, "Surface modification of metals by high power lasers," Surface and Coatings Technology, vol. 100–101, 1998, pp. 377–382.

[3] S. C. Tam, R. Williams, L. J. Yang, S. Jana, L. E. N. Lim, M. W. S. Lau, "A review of the laser processing of aircraft components," Journal of Materials Processing Technology, vol. 23, 1990, pp. 177–194.

[4] P. Hoffmann, M. Geiger, "Recent developments in laser system technology for welding applications," Annals of the CIRP, vol. 44, no. 1, 1995, pp. 151–156.

[5]P. D. Pietro, Y. L. Yao, "An investigation into characterizing and optimizing laser cutting quality," International Journal of Machine Tools & Manufacture, vol. 34, no. 2, 1994, pp. 225–243.

[6] A. K. Dubey, V. Yadava, "Laser beam machining—A review," International Journal of Machine Tools and Manufacture, vol. 48, no. 6, 2008, pp. 609–628.

[7] H. W. Bergmann, K. Schutte, E. Schubert, A. Emmel, "Laser-surface processing of metals and ceramics for industrial applications," Applied Surface Science, vol. 86, 1995, pp. 259–265.

[8] L. Zhao, Z. Tian, Y. Peng, "Microstructure and mechanical properties of heat-affected zone of high nitrogen steel simulated for laser welding conditions," ISIJ International, vol. 47, no. 9, 2007, pp. 1351–1356.

[9] K. Esterling, Introduction to the Physical Metallurgy of Welding, Butterworths& Co Ltd., Sevenoaks, 1983.

[10] S. Kou, Welding metallurgy, 2nd ed., John Wiley & Sons, Inc., Hoboken, New Jersey, 2003.

[11] S. Valette, E. Audouard, R. L. Harzic, N. Huot, "Heat affected zone in aluminum single crystals submitted to femtosecond laser

irradiations," Applied Surface Science, vol. 239, 2005, pp. 381–386.
[12] R. Singh, M. J. Alberts, S. N. Melkote, "Characterization and prediction of the heat-affected zone in a laser-assisted mechanical micromachining process," International Journal of Machine Tools & Manufacture, vol. 48, 2008, pp. 994–1004.
[13] K. Y. Benyounis, A. G. Olabi, M. S. J. Hashmi, "Effect of laser welding parameters on the heat input and weld-bead profile," Journal of Materials Processing Technology, vol. 165, 2005, pp. 978–985.
[14] F. Kong, S. Santhanakrishnan, D. Lin, R. Kovacevic, "Modeling of temperature field and grain growth of a dual phase steel DP980 in direct diode laser heat treatment," Journal of Materials Processing Technology, vol. 209, 2009, pp. 5996–6003.
[15] J. Yang, S. Sun, M. Brandt, W. Yan, "Experimental investigation and 3D finite element prediction of the heat affected zone during laser assisted machining of Ti6Al4V alloy," Journal of Materials Processing Technology, vol. 210, no. 15, 2010, pp. 2215–2222.
[16] R. G. Thiessen, I. M. Richardson, "A physically based model for microstructure development in a macroscopic heat affected zone: Grain growth and recrystallization," Metallurgical and Materials Transactions A, vol. 37B, 2006, pp. 655–663.
[17] W. J. Boettinger, J. A. Warren, C. Beckermann, A. Karma, "Phase field simulation of solidification," Annual Review Materials Research, vol. 32, no. 1, 2002, pp. 63–94.
[18] H. Assadi, "A phase-field model for crystallization into multiple grain structures," in Solidification and Crystallization, D. M. Herlach (Ed.), Wiley–VCH, Weinheim, 2004, pp. 17–26.
[19] I. Hadi, M.A. Jabbareh, R. Nikbakht, H. Assadi, "Modelling of microstructure evolution during thermal processes – a hybrid deterministic-probabilistic approach," Materials Science Forum, vol. 704–705, 2012, pp. 63–70.
[20] C. S. Pande, E. Dantsker, "On a stochastic theory of grain growth-III," ActaMetallurgicaetMaterialia, vol. 39, no. 6, 1991, pp. 1359–1365.
[21] Z. Yang, S. Sista, J. W. Elmer, T. Debroy, "Three Dimensional Monte Carlo Simulation of Grain Growth During GTA Welding of Titanium," ActaMetallurgica, vol. 48, no. 1359, 2000, pp. 4813–4825.
[22] H. Ikawa, S. Shin, H. Oshige, "Grain growth of commercial pure nickel in weld heat affected zone," transactions of the japan welding society, vol. 6, no. 1, 1975, pp. 17–22.